Journal of Zhejiang University-SCIENCE A (Applied Physics & Engineering)
ISSN 1673-565X (Print); ISSN 1862-1775 (Online)
www.zju.edu.cn/jzus; www.springerlink.com
E-mail: jzus@zju.edu.cn

Vertical vibration of a large diameter pile embedded in inhomogeneous soil based on the Rayleigh-Love rod theory*

Zhen-ya LI[1,2], Kui-hua WANG[†‡1,2], Wen-bing WU[3], Chin Jian LEO[4]

([1]*MOE Key Laboratory of Soft Soils and Geoenvironmental Engineering, Zhejiang University, Hangzhou 310058, China*)

([2]*Research Central of Coastal Urban Geotechnical Engineering, Zhejiang University, Hangzhou 310058, China*)

([3]*Engineering Faculty, China University of Geosciences, Wuhan 430074, China*)

([4]*School of Computing, Engineering and Mathematics, University of Western Sydney, Penrith, Sydney, NSW 2751, Australia*)

[†]E-mail: zdwkh0618@zju.edu.cn

Received Dec. 24, 2015; Revision accepted June 14, 2016; Crosschecked Nov. 10, 2016

Abstract: The vertical vibration of a large diameter pile embedded in inhomogeneous soil with hysteretic type damping is investigated based on the 3D axisymmetric model. Firstly, the pile is assumed to be a Rayleigh-Love rod with the consideration of its transverse inertia effect. Following this assumption, the pile-soil system is divided into several segments according to the stratification of the surrounding soil, and the dynamic interactions of the adjacent soil layers are simulated using the distributed Voigt model. Meanwhile, the surrounding soil is discretized into finite annular vertical zones to consider its radial inhomogeneity, and the force equilibrium and displacement coordination are satisfied at the interfaces of the adjacent soil zones and the interface of the pile-soil. Then, the analytical solution in the frequency domain and the semi-analytical solution in the time domain are obtained by solving the vibration governing equations of pile-soil system. Based on the solutions, a parametric analysis is conducted to investigate the influence of the transverse inertia effect on the dynamic response of the large diameter pile and its relationship with the pile parameters and the radial inhomogeneity of the surrounding soil. Finally, a comparison with the measured result and two other calculated results is presented to verify the effectiveness of the present solution.

Key words: Large diameter pile, Vertical vibration, Transverse inertia effect, Rayleigh-Love rod model, Inhomogeneous soil
http://dx.doi.org/10.1631/jzus.A1500341 **CLC number:** TU471.3

1 Introduction

The pile vibration theory, which takes the dynamic response of a pile subjected to a dynamic loading as the research object, can provide valuable references for the aseismic design and integrity detection of the pile. In light of this, much attention has been attracted to the study of the dynamic response of piles and various kinds of pile-soil dynamic interaction models have been put forward in the past decades, such as the Kelvin-Voigt model (Nogami and Konagai, 1988; Yesilce and Catal, 2008a; 2008b; 2008c; Ding *et al.*, 2011; Wu *et al.*, 2012; Li *et al.*, 2015), plane-strain model (El Naggar and Novak, 1994; Han and Sabin, 1995; Militano and Rajapakse, 1999; Wang *et al.*, 2013), and 3D axisymmetric model (Nogami and Novák, 1976; Zhou *et al.*, 2009; Wu *et al.*, 2013; 2014; Lü *et al.*, 2014; 2015). In the Kelvin-Voigt model, the interaction at the pile-soil interface is simulated by a linear spring and a dashpot connected in parallel, which is far from accurate when simulating the radial inhomogeneity of the soil as the parameters are assigned based on the experience. In the plane-strain model, the surrounding soil is assumed to consist of a series of infinite thin layers and the stress gradient is neglected. In the 3D

‡ Corresponding author

* Project supported by the National Natural Science Foundation of China (Nos. 51378464, 51579217, and 51309207)

ORCID: Zhen-ya LI, http://orcid.org/0000-0002-6671-0326; Kui-hua WANG, http://orcid.org/0000-0002-9362-0326

axisymmetric model, the wave effect of the surrounding soil is considered, in addition, the introduction of the fictitious soil pile model makes it possible to consider more complicated conditions of pile end soil (Wu *et al.*, 2014; Lü *et al*., 2015), which makes the model more accurate than the other two types.

At present, large diameter piles are widely used to provide greater bearing capacity. For this type of pile, the pile vibration theory developed on the basis of the 1D wave theory is not applicable because of its small slenderness ratio and obvious 3D effect of wave propagation. Previous studies have shown that the 1D solution from the numerical analysis for the large diameter pile is unsatisfactory in the comparison with the measured result because of the wave dispersion effect (Liao and Roesset, 1997; Chow *et al.*, 2003; Seidel and Tan, 2004; Chai *et al.*, 2010; 2011).

Given this, the Rayleigh-Love rod model was proposed by some researchers to simulate the large diameter pile and satisfactory results have been gained. In this model, the transverse inertia effect of the pile is considered to approximately take account of the 3D effect of the wave propagation. By means of the saturated soil theory presented by Biot and the Rayleigh-Love rod theory, Li *et al*. (2005) investigated the longitudinal vibration of a large diameter end-bearing pile embedded in homogeneous saturated soil and pointed out that the calculated result which allows for the transverse inertia effect of the pile is in a better agreement with the field pile dynamic test result. Assuming the rock-socketed large diameter pile to be a Rayleigh-Love rode, Yu *et al*. (2013) analyzed the influence of the sediment on the dynamic impedance at the pile head. Lü *et al.* (2014) used this model to investigate the dynamic response of a pile embedded in multilayered soil and compared the influence of the transverse inertia effect on the longitudinal vibration of the intact pile and the defective pile. Lü *et al.* (2015) also studied the relationship between the transverse inertia effect and the pile end soil by introducing the fictitious soil pile model into the solution. Yang and Tang (2013) used this model to investigate the dynamic response of large diameter piles. The solution proposed by Li *et al*. (2005) only deals with the homogeneous soil, which is not applicable in most practical engineering given the complicated engineering geological conditions. Some progress was made by Yang and Tang (2013), Yu *et al*. (2013), and Lü *et al*. (2014; 2015), as the layered properties of the surrounding soil were considered, but the pile-soil interaction model by Yang and Tang (2013) and Yu *et al*. (2013) was too simple.

Another main difference between the large diameter pile and the slender pile is the construction disturbance effect, which makes the surrounding soil inhomogeneous in the radial direction (Elkasabgy and El Naggar, 2013; Jardine *et al.*, 2013; Zhou *et al.*, 2013; 2015). This phenomenon not only affects the bearing capacity of the pile (El Naggar and Wei, 2000; Liu *et al*., 2010; Gong *et al*., 2012; He *et al*., 2015), but also has an impact on the dynamic behavior of the pile (Han, 1997; El Naggar, 2000; Yang and Tang, 2013; Tian *et al.*, 2015).

It can be seen that the radial inhomogeneity of the surrounding soil caused by the construction disturbance effect is an important factor that should be considered in the dynamic response analysis of the large diameter pile. However, the earlier works mentioned above can only deal with the homogeneous or horizontally layer-wise homogeneous soil. This limitation makes them unable to fully simulate the actual engineering condition as the radial inhomogeneity of the soil is not considered. In light of this, an improved solution is proposed in this paper to investigate the vertical vibration of a large diameter pile embedded in inhomogeneous soil. The Rayleigh-Love rod model is used to consider the transverse inertia effect of the pile, a 3D axisymmetric model which only considers the vertical displacement field of the surrounding soil is adopted to build a pile-soil interaction model, and the shear complex stiffness transfer method is employed to simulate the radial inhomogeneity of the surrounding soil. Then, based on the parametric analysis, the influence of the inertia effect on the dynamic response of the pile, and its relationship with pile parameters and the radial inhomogeneity of the soil, are revealed.

2 Calculation model and governing equations

2.1 Calculation model

As shown in Fig. 1, the pile-soil system is divided into n segments in the vertical direction and the

surrounding soil is discretized into m vertical annular zones in the radial direction to consider the vertical and radial inhomogeneity of soil, respectively. l and $q(t)$ are the pile length and the vertical harmonic force acting on the pile head, respectively. l_i and h_i are the thickness and the depth of the upper interface of the ith pile segment, respectively. $r_{i,k}$ denotes the inner radius of the kth soil zone within the ith layer. The contact traction acting on the kth soil zone within the ith layer due to the adjacent soil layers is denoted by disturbed Voigt model, where $k_{i+1,k}$ and $k_{i,k}$ denote the spring constants, and $\delta_{i+1,k}$ and $\delta_{i,k}$ represent the damping coefficients. The pile end soil is simulated by a single Voigt model with a spring constant of k_b and a damping coefficient of δ_b. According to Randolph and Deeks (1992), $k_\mathrm{b}=8G_\mathrm{b}^\mathrm{s}\Big/\left[\pi\left(1-\mu_\mathrm{b}^\mathrm{s}\right)d\right]$, $\delta_\mathrm{b}=3.2G_\mathrm{b}^\mathrm{s}\Big/\left[\pi\left(1-\mu_\mathrm{b}^\mathrm{s}\right)v_\mathrm{b}^\mathrm{s}\right]$, where $\mu_\mathrm{b}^\mathrm{s}$, v_b^s, $G_\mathrm{b}^\mathrm{s}=\rho_\mathrm{b}^\mathrm{s}(v_\mathrm{b}^\mathrm{s})^2$, and $\rho_\mathrm{b}^\mathrm{s}$ represent Poisson's ratio, shear wave velocity, shear modulus, and mass density of the pile end soil, respectively, whereas d is the diameter of the pile.

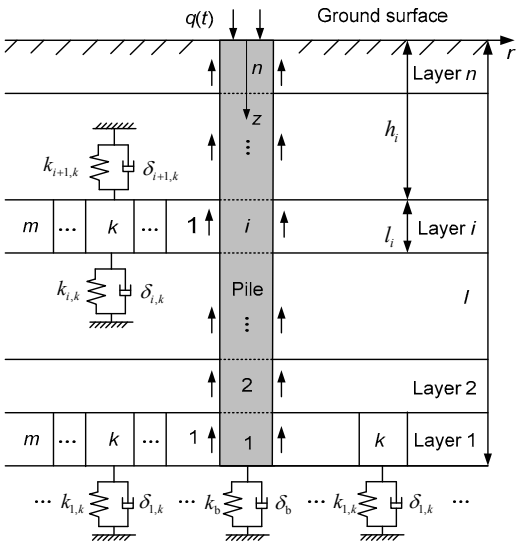

Fig. 1 Schematic of pile-soil model

2.2 Assumptions

1. The pile is viscoelastic, circular in cross section, and is simulated by the Rayleigh-Love rod model.

2. The outmost soil zone is infinite in the radial direction. The soil medium of the same annular zone within the same layer is homogeneous, but may vary from zone to zone or layer to layer. The shear stress equilibrium and the displacement continuity are satisfied at the interfaces of the adjacent soil annular zones.

3. The free top surface of the surrounding soil has no normal or shear stress. Only the vertical displacement of the soil is considered.

4. The soil-pile system is subjected to small deformations and strains and has a perfect contact during the vibration.

3 Governing equations and solutions

3.1 Governing equation of the soil and its solution

Based on the 3D axisymmetric model, which only considers the vertical displacement of soil, the dynamic vibration equation of soil proposed by Nogami and Novák (1976) is adopted herein:

$$\begin{aligned}&\left[\left(\lambda_{i,k}^\mathrm{s}+2G_{i,k}^\mathrm{s}\right)+\mathrm{i}\left(\lambda_{i,k}'+2G_{i,k}'\right)\right]\frac{\partial^2}{\partial z^2}u_{i,k}^\mathrm{s}(r,z,t)\\&+\left(G_{i,k}^\mathrm{s}+\mathrm{i}G_{i,k}'\right)\left(\frac{1}{r}\frac{\partial}{\partial r}+\frac{\partial^2}{\partial r^2}\right)u_{i,k}^\mathrm{s}(r,z,t)\\&=\rho_{i,k}^\mathrm{s}\frac{\partial^2}{\partial t^2}u_{i,k}^\mathrm{s}(r,z,t),\end{aligned}\tag{1}$$

where $u_{i,k}^\mathrm{s}(r,z,t)$, $\lambda_{i,k}^\mathrm{s}=E_{i,k}^\mathrm{s}\mu_{i,k}^\mathrm{s}/[(1+\mu_{i,k}^\mathrm{s})(1-2\mu_{i,k}^\mathrm{s})]$, and $G_{i,k}^\mathrm{s}=\rho_{i,k}^\mathrm{s}(v_{i,k}^\mathrm{s})^2$ represent the vertical displacement, Lame's elastic constant, and shear modulus of the kth soil zone within the ith layer, respectively; $E_{i,k}^\mathrm{s}=\rho_{i,k}^\mathrm{s}(c_{i,k}^\mathrm{s})^2$, $\mu_{i,k}^\mathrm{s}$, $\rho_{i,k}^\mathrm{s}$, $c_{i,k}^\mathrm{s}$, and $v_{i,k}^\mathrm{s}$ are the elastic modulus, Poisson's ratio, mass density, longitudinal wave velocity, and shear wave velocity of the kth soil zone within the ith layer, respectively; $\lambda_{i,k}'$ and $G_{i,k}'$ are the viscosity coefficients of the Lame's elastic constant and shear modulus, respectively; $\mathrm{i}=\sqrt{-1}$.

According to Yang *et al.* (2013), the equation of the soil zones can be solved from the outer to inner zone, and the vertical displacement of the kth soil

zone within the *i*th layer can be obtained as

$$U_{i,k}^{\mathrm{s}}=\begin{cases}\sum_{j=1}^{\infty}A_{i,kj}K_0\left(\gamma_{i,kj}r\right)\cos\left(\beta_{i,kj}z'-\varphi_{i,kj}\right), & k=m,\\ \sum_{j=1}^{\infty}\left[B_{i,kj}I_0\left(\gamma_{i,kj}r\right)+C_{i,kj}K_0\left(\gamma_{i,kj}r\right)\right]\\ \quad\times\cos\left(\beta_{i,kj}z'-\varphi_{i,kj}\right), & k=1,2,\ldots,m-1,\end{cases}\tag{2}$$

where $U_{i,k}^{\mathrm{s}}=U_{i,k}^{\mathrm{s}}(r,z,s)$ is the Laplace transform of $u_{i,k}^{\mathrm{s}}(r,z,t)$ with respect to time t; $z'=z-h_i$; $I_0\left(\gamma_{i,kj}r\right)$ and $K_0\left(\gamma_{i,kj}r\right)$ denote the modified Bessel functions of order zero of the first and second kinds, respectively; $A_{i,kj}$, $B_{i,kj}$, and $C_{i,kj}$ are constants which can be determined by boundary conditions; $\gamma_{i,kj}^2=\dfrac{\left\{\xi_{i,k}^2+\mathrm{i}\left[\eta_{\mathrm{v}i,k}\left(\xi_{i,k}^2-2\right)+2\eta_{si,k}\right]\right\}\beta_{i,kj}^2-\left(\omega/v_{i,k}^{\mathrm{s}}\right)^2}{1+\mathrm{i}\eta_{si,k}}$; $\xi_{i,k}=c_{i,k}^{\mathrm{s}}/v_{i,k}^{\mathrm{s}}=\sqrt{2\left(1-\mu_{i,k}^{\mathrm{s}}\right)/\left(1-2\mu_{i,k}^{\mathrm{s}}\right)}$; $\eta_{si,k}=G'_{i,k}/G_{i,k}^{\mathrm{s}}$ and $\eta_{\mathrm{v}i,k}=\lambda'_{i,k}/\lambda_{i,k}^{\mathrm{s}}$ are the hysteretic-type damping for any frequency; ω is the circular frequency; $\tan\left(\beta_{i,kj}l_i\right)=\left[\left(\overline{K_{i,k}}+\overline{K'_{i,k}}\right)\beta_{i,kj}l_i\right]\Big/\left[\left(\beta_{i,kj}l_i\right)^2-\overline{K_{i,k}}\,\overline{K'_{i,k}}\right]$, $\varphi_{i,kj}=\arctan\left(\overline{K'_{i,k}}\Big/\left(\beta_{i,kj}l_i\right)\right)$; $\overline{K_{i,k}}=(k_{i,k}+\mathrm{i}\omega\delta_{i,k})l_i/E_{i,k}^{\mathrm{s}}$ and $\overline{K'_{i,k}}=(k_{i+1,k}+\mathrm{i}\omega\delta_{i+1,k})l_i/E_{i,k}^{\mathrm{s}}$ denote the dimensionless complex stiffness at the bottom and the top of the *k*th soil zone within the *i*th layer, respectively.

The shear stress of the interface between the *k*th and the (*k*−1)th soil zones can be given as

$$\tau_{i,k}^{\mathrm{s}}=\begin{cases}-G_{i,k}^{\mathrm{s}}\left(1+\mathrm{i}\eta_{si,k}\right)\\ \quad\times\sum_{j=1}^{\infty}A_{i,kj}\gamma_{i,kj}K_1\left(\gamma_{i,kj}r_{i,k}\right)\cos\left(\beta_{i,kj}z'-\varphi_{i,kj}\right), & k=m,\\ G_{i,k}^{\mathrm{s}}\left(1+\mathrm{i}\eta_{si,k}\right)\\ \quad\times\sum_{j=1}^{\infty}\left\{\left[B_{i,kj}\gamma_{i,kj}I_1\left(\gamma_{i,kj}r_{i,k}\right)-C_{i,kj}\gamma_{i,kj}K_1\left(\gamma_{i,kj}r_{i,k}\right)\right]\right.\\ \qquad\left.\times\cos\left(\beta_{i,kj}z'-\varphi_{i,kj}\right)\right\}, & k=1,2,\ldots,m-1,\end{cases}\tag{3}$$

where $I_1\left(\gamma_{i,kj}r_{i,k}\right)$ and $K_1\left(\gamma_{i,kj}r_{i,k}\right)$ are the modified Bessel functions of order one of the first and second kinds, respectively; according to Yang *et al.* (2013), the ratio of $B_{i,kj}$ to $C_{i,kj}$, which is denoted by $M_{i,kj}$ in this study, can be obtained based on the continuity of the displacements and stresses at the interfaces of adjacent soil zones.

3.2 Governing equation of the pile and its solution

From the energetic standpoint, Rayleigh and Love deduced a governing equation (referred as the Rayleigh-Love equation), to approximately take account of the 3D effect of the wave propagation (Achenbach, 1973). From the Rayleigh-Love equation, the relationship between the wave velocity when considering the transverse inertia effect and that of the 1D theory can be obtained and approximately expressed as $c=c_0[1-(\mu^{\mathrm{p}}r^{\mathrm{p}}\zeta)^2]/4$, where c and c_0 denote the wave velocity when considering the transverse inertia effect and that of the 1D theory; μ^{p}, r^{p}, and ζ represent Poisson's ratio, radius, and circular wavenumber, respectively. It can be seen that the wave velocity decreases compared with that of the 1D theory, which means the time lag of the reflected signals for the same pile length. This phenomenon will be discussed in Section 4. Based on the Rayleigh-Love rod theory, and taking the material damping of pile and the reaction of soil into account, the vertical vibration of the *i*th pile segment can be obtained as

$$\begin{aligned}&E_i^{\mathrm{p}}A_i^{\mathrm{p}}\frac{\partial^2}{\partial z^2}u_i^{\mathrm{p}}(z,t)+A_i^{\mathrm{p}}\delta_i^{\mathrm{p}}\frac{\partial^3}{\partial z^2\partial t}u_i^{\mathrm{p}}(z,t)\\ &-\rho_i^{\mathrm{p}}A_i^{\mathrm{p}}\left[\frac{\partial^2}{\partial t^2}u_i^{\mathrm{p}}(z,t)-\left(\mu_i^{\mathrm{p}}r_i^{\mathrm{p}}\right)^2\frac{\partial^4}{\partial z^2\partial t^2}u_i^{\mathrm{p}}(z,t)\right]\\ &-2\pi r_{i,1}f_i\left(r_{i,1},z,t\right)=0,\end{aligned}\tag{4}$$

where $f_i(r_{i,1},z,t)=-\tau_{i,1}^{\mathrm{s}}\big|_{r=r_{i,1}}=-G_{i,1}^{\mathrm{s}}(1+\mathrm{i}\eta_{si,1})\dfrac{\partial}{\partial r}u_{i,1}^{\mathrm{s}}\big|_{r=r_{i,1}}$ is the frictional force acting on the surface of the *i*th pile segment, $\tau_{i,1}^{\mathrm{s}}$ is the shear stress of the pile-soil interface, $E_i^{\mathrm{p}}=\rho_i^{\mathrm{p}}(c_i^{\mathrm{p}})^2$, $A_i^{\mathrm{p}}=\pi(r_i^{\mathrm{p}})^2$, c_i^{p}, δ_i^{p}, and μ_i^{p} denote the elastic modulus, cross sectional area, longitudinal wave velocity, material damping, and

Poisson's ratio of the *i*th pile segment, respectively. $u_i^{\mathrm{p}}(z,t)$ is the vertical displacement of the *i*th pile segment.

Allowing for the continuity conditions of the vertical displacement and axial force at the interface of the pile segment, boundary conditions at the top and bottom of the *i*th pile segment can be given as

$$\left[\left(E_i^{\mathrm{p}}A_i^{\mathrm{p}}+A_i^{\mathrm{p}}\delta_i^{\mathrm{p}}\frac{\partial}{\partial t}\right)\frac{\partial u_i^{\mathrm{p}}}{\partial z}+\rho_i^{\mathrm{p}}A_i^{\mathrm{p}}\left(\mu_i^{\mathrm{p}}r_i^{\mathrm{p}}\right)^2\frac{\partial^3 u_i^{\mathrm{p}}}{\partial z\partial t^2}+z_i^{\mathrm{p}}u_i^{\mathrm{p}}\right]\Bigg|_{z=h_i}=0, \tag{5}$$

$$\left[\left(E_i^{\mathrm{p}}A_i^{\mathrm{p}}+A_i^{\mathrm{p}}\delta_i^{\mathrm{p}}\frac{\partial}{\partial t}\right)\frac{\partial u_i^{\mathrm{p}}}{\partial z}+\rho_i^{\mathrm{p}}A_i^{\mathrm{p}}\left(\mu_i^{\mathrm{p}}r_i^{\mathrm{p}}\right)^2\frac{\partial^3 u_i^{\mathrm{p}}}{\partial z\partial t^2}+z_{i-1}^{\mathrm{p}}u_i^{\mathrm{p}}\right]\Bigg|_{z=h_i+l_i}=0, \tag{6}$$

where z_i^{p} and z_{i-1}^{p} represent the displacement impedance functions at the top and bottom of the *i*th pile segment, and their Laplace transforms are Z_i^{p} and Z_{i-1}^{p}, respectively.

Based on the continuity conditions of the displacement and stress at the *i*th pile-soil interface, one obtains:

$$u_i^{\mathrm{p}}(z,t)=u_{i,1}^{\mathrm{s}}\left(r_{i,1},z,t\right), \tag{7}$$

$$f_i\left(r_{i,1},z,t\right)=-\tau_{i,1}^{\mathrm{s}}\big|_{r=r_{i,1}}. \tag{8}$$

The initial displacement and initial velocity of the *i*th pile segment can be given as

$$\begin{cases}u_i^{\mathrm{p}}(z,t)\big|_{t=0}=0,\\ \dfrac{\partial u_i^{\mathrm{p}}(z,t)}{\partial t}\Big|_{t=0}=0.\end{cases} \tag{9}$$

Substituting Eqs. (3) and (8) into Eq. (4) and reducing it gives

$$\left(c_i^{\mathrm{p}}\right)^2\left[1+\frac{\delta_i^{\mathrm{p}}\mathrm{i}\omega}{E_i^{\mathrm{p}}}-\frac{\left(\mu_i^{\mathrm{p}}r_i^{\mathrm{p}}\right)^2\omega^2}{\left(c_i^{\mathrm{p}}\right)^2}\right]\frac{\partial^2 U_i^{\mathrm{p}}}{\partial(z')^2}+\omega^2U_i^{\mathrm{p}}+\frac{2\pi r_{i,1}G_{i,1}^{\mathrm{s}}\left(1+\mathrm{i}\eta_{si,1}\right)}{\rho_i^{\mathrm{p}}A_i^{\mathrm{p}}}\times\sum_{j=1}^{\infty}\left\{\left[B_{i,1j}\gamma_{i,1j}I_1\left(\gamma_{i,1j}r_{i,1}\right)-C_{i,1j}\gamma_{i,1j}K_1\left(\gamma_{i,1j}r_{i,1}\right)\right]\times\cos\left(\beta_{i,1j}z'-\varphi_{i,1j}\right)\right\}=0, \tag{10}$$

where $U_i^{\mathrm{p}}=U_i^{\mathrm{p}}(z',s)$ represents the Laplace transform of $u_i^{\mathrm{p}}(z',t)$ with respect to time *t*.

By solving Eq. (10), one obtains:

$$U_i^{\mathrm{p}}=D_i\cos\left(\frac{\overline{\lambda_i}}{l_i}z'\right)+D_i'\sin\left(\frac{\overline{\lambda_i}}{l_i}z'\right)+\sum_{j=1}^{\infty}N_{ij}\cos\left(\beta_{i,1j}z'-\varphi_{i,1j}\right), \tag{11}$$

where $\overline{\lambda_i}$ is the dimensionless parameter, i.e.,

$$\overline{\lambda_i}=\sqrt{\omega^2t_i^2\Big/\left[1+\delta_i^{\mathrm{p}}\mathrm{i}\omega/E_i^{\mathrm{p}}-\left(\mu_i^{\mathrm{p}}r_i^{\mathrm{p}}\right)^2\omega^2\Big/\left(c_i^{\mathrm{p}}\right)^2\right]},$$

$$N_{ij}=-\frac{2\pi r_{i,1}G_{i,1}^{\mathrm{s}}\left(1+\mathrm{i}\eta_{si,1}\right)}{\rho_i^{\mathrm{p}}A_i^{\mathrm{p}}}\times\frac{B_{i,1j}\gamma_{i,1j}I_1\left(\gamma_{i,1j}r_{i,1}\right)-C_{i,1j}\gamma_{i,1j}K_1\left(\gamma_{i,1j}r_{i,1}\right)}{\omega^2-\left(c_i^{\mathrm{p}}\beta_{i,1j}\right)^2\omega^2t_i^2\Big/\overline{\lambda_i}^2}.$$

According to Eq. (7),

$$\sum_{j=1}^{\infty}\left[B_{i,1j}I_0\left(\gamma_{i,1j}r_{i,1}\right)+C_{i,1j}K_0\left(\gamma_{i,1j}r_{i,1}\right)\right]\times\cos\left(\beta_{i,1j}z'-\varphi_{i,1j}\right)=D_i\cos\left(\frac{\overline{\lambda_i}}{l_i}z'\right)+D_i'\sin\left(\frac{\overline{\lambda_i}}{l_i}z'\right)+\sum_{j=1}^{\infty}N_{ij}\cos\left(\beta_{i,1j}z'-\varphi_{i,1j}\right). \tag{12}$$

From Eqs. (11) and (12), together with the orthogonality of the eigenfunction $\cos\left(\beta_{i,1j}z'-\varphi_{i,1j}\right)$ (*j*=1, 2, …) on the interval $\left[0,l_i\right]$, the displacement of the *i*th pile segment can be obtained:

$$U_i^{\mathrm{p}}=D_i\left[\cos\left(\frac{\overline{\lambda_i}}{l_i}z'\right)+\sum_{j=1}^{\infty}\chi_{ij}'\cos\left(\beta_{i,1j}z'-\varphi_{i,1j}\right)\right]$$

$$+D_i'\left[\sin\left(\frac{\overline{\lambda_i}}{l_i}z'\right)-\sum_{j=1}^{\infty}\chi_{ij}''\cos\left(\beta_{i,1j}z'-\varphi_{i,1j}\right)\right], \quad (13)$$

where

$$\chi_{ij}'=\chi_{ij}\left[\frac{\sin\left[\left(\overline{\lambda_i}-\overline{\beta_{i,1j}}\right)+\varphi_{i,1j}\right]-\sin\left(\varphi_{i,1j}\right)}{\overline{\lambda_i}-\overline{\beta_{i,1j}}}+\frac{\sin\left[\left(\overline{\lambda_i}+\overline{\beta_{i,1j}}\right)-\varphi_{i,1j}\right]+\sin\left(\varphi_{i,1j}\right)}{\overline{\lambda_i}+\overline{\beta_{i,1j}}}\right],$$

$$\chi_{ij}''=\chi_{ij}\left[\frac{\cos\left[\left(\overline{\lambda_i}+\overline{\beta_{i,1j}}\right)-\varphi_{i,1j}\right]-\cos\left(\varphi_{i,1j}\right)}{\overline{\lambda_i}+\overline{\beta_{i,1j}}}+\frac{\cos\left[\left(\overline{\lambda_i}-\overline{\beta_{i,1j}}\right)+\varphi_{i,1j}\right]-\cos\left(\varphi_{i,1j}\right)}{\overline{\lambda_i}-\overline{\beta_{i,1j}}}\right],$$

$$\chi_{ij}=-\frac{\overline{\rho_{i,1}^{\mathrm{s}}}\,\overline{v_{i,1}^{\mathrm{s}}}^{2}\left(1+\mathrm{i}\eta_{si,1}\right)\overline{\gamma_{i,1j}}}{\overline{r_i^{\mathrm{p}}}\left(\theta_i^2-\dfrac{\overline{\beta_{i,1j}}^{2}\theta_i^2}{\overline{\lambda_i}^{2}}\right)\phi_{ij}L_{ij}}\times\left[M_{i,1j}I_1\left(\gamma_{i,1j}r_i^{\mathrm{p}}\right)-K_1\left(\gamma_{i,1j}r_i^{\mathrm{p}}\right)\right],$$

$$L_{ij}=\int_0^{l_i}\cos^2\left(\beta_{i,1j}z'-\varphi_{i,1j}\right)\mathrm{d}z',$$

$$\phi_{ij}=M_{i,1j}\left[I_0\left(\gamma_{i,1j}r_i^{\mathrm{p}}\right)+\frac{2\overline{\rho_{i,1}^{\mathrm{s}}}\,\overline{v_{i,1}^{\mathrm{s}}}^{2}\left(1+\mathrm{i}\eta_{si,1}\right)\overline{\gamma_{i,1j}}}{\overline{r_i^{\mathrm{p}}}\left(\theta_i^2-\dfrac{\overline{\beta_{i,1j}}^{2}\theta_i^2}{\overline{\lambda_i}^{2}}\right)}I_1\left(\gamma_{i,1j}r_i^{\mathrm{p}}\right)\right]+K_0\left(\gamma_{i,1j}r_i^{\mathrm{p}}\right)-\frac{2\overline{\rho_{i,1}^{\mathrm{s}}}\,\overline{v_{i,1}^{\mathrm{s}}}^{2}\left(1+\mathrm{i}\eta_{si,1}\right)\overline{\gamma_{i,1j}}}{\overline{r_i^{\mathrm{p}}}\left(\theta_i^2-\dfrac{\overline{\beta_{i,1j}}^{2}\theta_i^2}{\overline{\lambda_i}^{2}}\right)}K_1\left(\gamma_{i,1j}r_i^{\mathrm{p}}\right).$$

$\theta_i=\omega t_i$, $\overline{\beta_{i,1j}}=\beta_{i,1j}l_i$, $\overline{\gamma_{i,1j}}=\gamma_{i,1j}l_i$, $\overline{v_{i,1}^{\mathrm{s}}}=v_{i,1}^{\mathrm{s}}/c_i^{\mathrm{p}}$, $\overline{\rho_{i,1}^{\mathrm{s}}}=\rho_{i,1}^{\mathrm{s}}/\rho_i^{\mathrm{p}}$, and $\overline{r_i^{\mathrm{p}}}=r_i^{\mathrm{p}}/l_i$ are all dimensionless parameters; t_i is the propagation time of the elastic wave in the ith pile segment.

Combining with the boundary conditions Eqs. (5) and (6), and together with the impedance function transfer method, the impedance function at the pile head (i=n) can be expressed as

$$Z_n^{\mathrm{p}}=-\frac{E_n^{\mathrm{p}}A_n^{\mathrm{p}}+A_n^{\mathrm{p}}\delta_n^{\mathrm{p}}\mathrm{i}\omega-\rho_n^{\mathrm{p}}A_n^{\mathrm{p}}\left(\mu_n^{\mathrm{p}}r_n^{\mathrm{p}}\right)^2\omega^2}{l_n}\times\frac{\dfrac{D_n}{D_n'}\sum_{j=1}^{\infty}\chi_{nj}'\overline{\beta_{n,1j}}\sin\varphi_{n,1j}+\overline{\lambda_n}-\sum_{j=1}^{\infty}\chi_{nj}''\overline{\beta_{n,1j}}\sin\varphi_{n,1j}}{\dfrac{D_n}{D_n'}\left(1+\sum_{j=1}^{\infty}\chi_{nj}'\cos\varphi_{n,1j}\right)-\sum_{j=1}^{\infty}\chi_{nj}''\cos\varphi_{n,1j}}, \quad (14)$$

where

$$\frac{D_n}{D_n'}=\left\{\frac{Z_{n-1}^{\mathrm{p}}l_n}{E_n^{\mathrm{p}}A_n^{\mathrm{p}}}\left[\sin\left(\overline{\lambda_n}\right)-\sum_{j=1}^{\infty}\chi_{nj}''\cos\left(\overline{\beta_{n,1j}}-\varphi_{n,1j}\right)\right]+\left[1+\frac{\delta_n^{\mathrm{p}}\mathrm{i}\omega}{E_n^{\mathrm{p}}}-\left(\mu_n^{\mathrm{p}}\overline{r_n^{\mathrm{p}}}\right)^2\theta_n^2\right]\times\left[\overline{\lambda_n}\sin\left(\overline{\lambda_n}\right)+\sum_{j=1}^{\infty}\chi_{nj}''\overline{\beta_{n,1j}}\sin\left(\overline{\beta_{n,1j}}-\varphi_{n,1j}\right)\right]\right\}\Bigg/\left\{-\frac{Z_{n-1}^{\mathrm{p}}l_n}{E_n^{\mathrm{p}}A_n^{\mathrm{p}}}\left[\cos\left(\overline{\lambda_n}\right)+\sum_{j=1}^{\infty}\chi_{nj}'\cos\left(\overline{\beta_{n,1j}}-\varphi_{n,1j}\right)\right]+\left[1+\frac{\delta_n^{\mathrm{p}}\mathrm{i}\omega}{E_n^{\mathrm{p}}}-\left(\mu_n^{\mathrm{p}}\overline{r_n^{\mathrm{p}}}\right)^2\theta_n^2\right]\times\left[\overline{\lambda_n}\sin\left(\overline{\lambda_n}\right)+\sum_{j=1}^{\infty}\chi_{nj}'\overline{\beta_{n,1j}}\sin\left(\overline{\beta_{n,1j}}-\varphi_{n,1j}\right)\right]\right\}.$$

Such that the frequency response function of the velocity at the pile head can be written as

$$H_{\mathrm{v}}(\omega)=-\frac{1}{\rho_n^{\mathrm{p}}A_n^{\mathrm{p}}c_n^{\mathrm{p}}}H_{\mathrm{v}}', \quad (15)$$

where

$$H_{\mathrm{v}}'=\frac{\mathrm{i}\theta_n}{1+\dfrac{\delta_n^{\mathrm{p}}\mathrm{i}\omega}{E_n^{\mathrm{p}}}-\left(\mu_n^{\mathrm{p}}\overline{r_n^{\mathrm{p}}}\right)^2\theta_n^2}\times\frac{\dfrac{D_n}{D_n'}\left(1+\sum_{j=1}^{\infty}\chi_{nj}'\cos\varphi_{n,1j}\right)-\sum_{j=1}^{\infty}\chi_{nj}''\cos\varphi_{n,1j}}{\dfrac{D_n}{D_n'}\sum_{j=1}^{\infty}\chi_{nj}'\overline{\beta_{n,1j}}\sin\varphi_{n,1j}+\overline{\lambda_n}-\sum_{j=1}^{\infty}\chi_{nj}''\overline{\beta_{n,1j}}\sin\varphi_{n,1j}},$$

which denotes the dimensionless frequency response function of the velocity.

In the nondestructive testing of pile, the excitation force is a half-sine pulse which can be expressed as $q(t)=Q_{\max}\sin(\pi t/T)$ $(t\in(0,T))$, where $Q_{\max}$ and T represent the amplitude and the impulse width of the excitation force, respectively, then the semi-analytical velocity response at the pile head can be obtained as

$$v(t)=-\frac{Q_{\max}}{\rho_n^{\mathrm{p}}A_n^{\mathrm{p}}c_n^{\mathrm{p}}}v'(t), \tag{16}$$

where $v'(t)=\frac{1}{2}\int_{-\infty}^{+\infty}\frac{H_{\mathrm{v}}'T}{\pi^2-T^2\omega^2}(1+\mathrm{e}^{-\mathrm{i}\omega t})\,\mathrm{e}^{\mathrm{i}\omega t}\mathrm{d}\omega$ denotes the dimensionless velocity response at the pile head.

4 Parametric study

Based on Eqs. (15) and (16), a parametric study is conducted to investigate the influence of the transverse inertia effect of the large diameter pile on the dynamic response at the pile head and its relationship with the pile parameters and the radial inhomogeneity of the surrounding soil.

Que and Wang (2007) and Lü *et al.* (2014) indicated that even changing within a comparatively large range, the influence of the Voigt model parameters at the interface of the soil layers on the dynamic response of the pile is still insignificant. As a result, the corresponding spring constants and damping coefficients in the following analysis are given values of 10000 N/m^3 and 10000 N/m^3·s, respectively.

4.1 Relationship between the transverse inertia effect and the pile parameters

To highlight the influence of the pile parameters, the soil is assumed to be homogeneous in this section. Pile-soil parameters are given in Table 1.

Table 1 Pile-soil parameters for the parametric study

Item	Value	
	Pile	Soil
Length (m)	10	
Radius (m)	0.5	
Density (kg/m^3)	2500	1800
Longitudinal wave velocity (m/s)	3600	
Shear wave velocity (m/s)		150
Poisson's ratio	0.2	0.4

4.1.1 Radius of the pile

In the following analysis, the pile radius is set to be r^{p}=0.25 m, 0.5 m, or 0.75 m. Poisson's ratio of the pile is μ^{p}=0 or 0.2, where μ^{p}=0 means that the transverse inertia effect of the pile is not considered. Other pile-soil parameters are given in Table 1.

The influences of the transverse inertia effect on the dynamic response at the pile head with different radiuses of the pile are shown in Fig. 2, where f and $t_0=t\Big/\sum_{i=1}^{n}t_i$ denote the frequency and the dimensionless time, respectively. As shown in Fig. 2a, the resonant frequencies of the velocity admittance decrease and the decrease rate increases as the frequency and pile radius increase when the transverse inertia effect is considered. In the frequency domain, the length of the pile can be calculated based on the relation $l=c^{\mathrm{p}}/(2\Delta f)$, where Δf is the frequency change between resonant peaks. As a result, the calculated pile length is longer than its actual value, and the error becomes more apparent for higher frequencies and larger pile radiuses. Fig. 2b shows that the amplitude decrease and width increase of the reflected signal from the pile tip can be observed when the transverse effect is taken into account. Meanwhile, the peak time of the reflected signal from the pile tip is delayed, making the calculated length of the pile longer than its actual value, which is consistent with the results reflected by Fig. 2a. In addition, the curve after the reflected signal is oscillating, while this phenomenon is imperceptible in the curve that neglects the transverse inertia effect of the pile. It can also be seen that the associated influences mentioned above become increasingly apparent with the increase of the pile radius.

4.1.2 Poisson's ratio of the pile

When investigating the influence of Poisson's ratio of the pile, μ^{p}=0, 0.15, 0.2, or 0.25, and the other parameters are the same as shown in Table 1.

Fig. 3 shows the influence of Poisson's ratio of the pile on the dynamic response at the pile head. It can be seen from Fig. 3a that the resonant frequencies of the velocity admittance decrease with the increase of Poisson's ratio of the pile, and the decreasing trend becomes more notable for higher frequencies. Fig. 3b

shows that as Poisson's ratio of the pile increases, the peak time of the reflected signal from the pile tip is gradually delayed, and the amplitude of the signal decreases, whereas the oscillation after the reflected signal from the pile tip becomes more apparent.

4.1.3 Concrete strength grade of the pile

The concrete strength grades and elastic modulus of the pile are given in Table 2 according to the national standard in China (MOHURD, 2010). In this section, the influence of the concrete strength grade is reflected by the longitudinal wave velocity calculated based on the relation $c^{\mathrm{p}}=\sqrt{E^{\mathrm{p}}/\rho^{\mathrm{p}}}$. Other pile-soil parameters are shown in Table 1.

The influences of the transverse inertia effect on the dynamic response at the pile head with different concrete strength grades of pile are shown in Fig. 4. It can be noted from Fig. 4a that when the transverse inertia effect is considered, the decrease of the resonant frequencies becomes less notable for higher concrete strength grades of the pile. Fig. 4b shows that as the concrete strength grade of the pile increases, the amplitude of the reflected signal from the pile tip increases, while the time lag of the reflected signal decreases. In conclusion, the influence of the transverse inertia effect weakens gradually as the concrete strength grade increases.

4.2 Influence of the radial inhomogeneity of the pile surrounding soil

4.2.1 Relationship between the transverse inertia effect and the radial inhomogeneity of the pile surrounding soil

The pile surrounding soil is radially inhomogeneous due to the construction disturbance effect. In this section, the relationship between the transverse inertia effect and the radial inhomogeneity of the pile surrounding soil is analyzed. The outer radius of the disturbed region is 0.5 m, the radial inhomogeneity of the surrounding soil is reflected by the change of the

Table 2 Concrete strength grades and the elastic modulus

Concrete strength grade	Elastic modulus (GPa)	Elastic wave velocity (m/s)
C20	25.5	3194
C40	32.5	3606
C60	36.0	3795

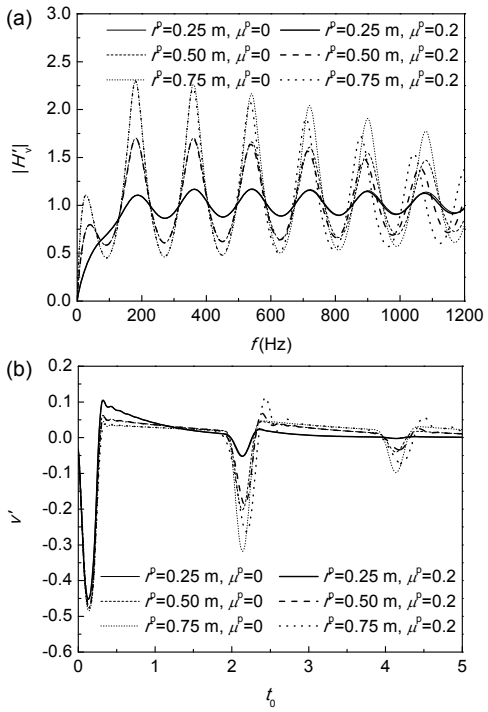

Fig. 2 Influence of the radius of the pile on the dynamic response at the pile head: (a) velocity admittance; (b) reflected wave signals

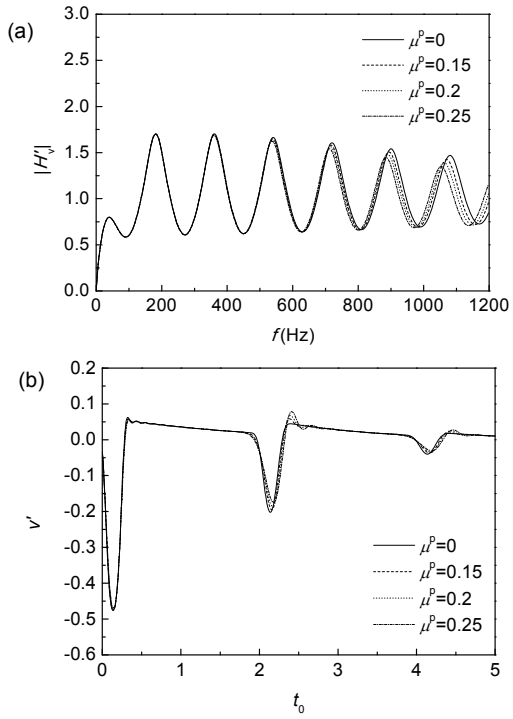

Fig. 3 Influence of Poisson's ratio of the pile on the dynamic response at the pile head: (a) velocity admittance; (b) reflected wave signal

parameters in the disturbed region (i.e., density and shear wave velocity) of three different cases: case 1 is that the soil parameters remain the same in the radial direction, namely the soil is homogeneous; case 2 and case 3 represent the strengthening and weakening of the surrounding soil, respectively. In the three cases, soil parameters are given as

Case 1: $\rho_k^s = 1800$ kg/m^3, $v_k^s = 150$ m/s;

Case 2: $\rho_k^s = \left[1800 + 100(m-k)/(m-1)\right]$ kg/m^3,

$v_k^s = \left[150 + 100(m-k)/(m-1)\right]$ m/s;

Case 3: $\rho_k^s = \left[1800 - 100(m-k)/(m-1)\right]$ kg/m^3,

$v_k^s = \left[150 - 100(m-k)/(m-1)\right]$ m/s.

Fig. 5 shows the influence of the transverse inertia effect on the dynamic response at the pile head when the radial inhomogeneity of the surrounding soil is considered. It can be seen from Fig. 5a that compared with the result for the radially homogeneous case, the oscillation amplitude of the velocity admittance decreases and the decreasing trend of the resonant frequencies decreases for the radially strengthened soil. However, the result is opposite for the soil weakening case. Fig. 5b shows that the reflected signal from the pile tip delays and its amplitude decreases for the soil strengthening case compared with the radially homogeneous case; moreover, the oscillation that appears immediately after the reflected signal tends to be imperceptible. The opposite phenomenon is observed for the weakened soil. Generally speaking, the radial inhomogeneity of the surrounding soil plays an important role in the dynamic characteristics of the pile as the influence of the transverse inertia effect can be weakened by the radially strengthening of the soil while strengthened by the weakening of the soil.

4.2.2 Influence of the strengthening degree of the surrounding soil

In this section, the soil parameters increase radially inwards from the outmost zone in three cases, viz. cases a, b, and c, in which the strengthening degree of the soil increases. The outer radius of the disturbed region is 0.5 m. In the three cases, parameters of each soil zone are given as

Case a: $\rho_k^s = \left[1800 + 50(m-k)/(m-1)\right]$ kg/m^3,

$v_k^s = \left[150 + 50(m-k)/(m-1)\right]$ m/s;

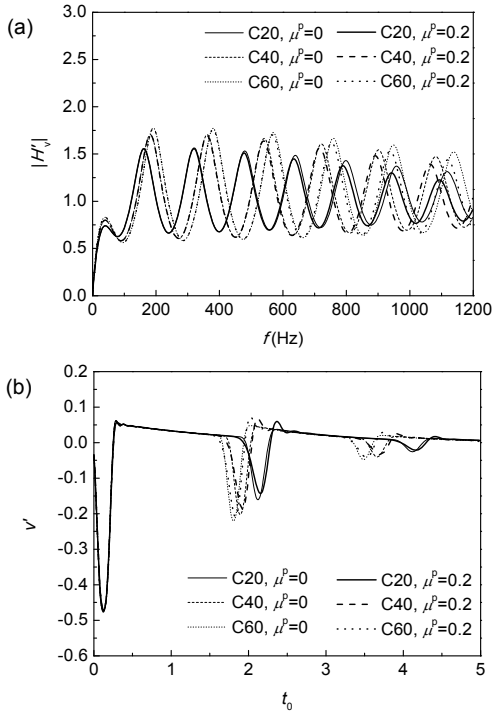

Fig. 4 Influence of the concrete strength grade of the pile on the dynamic response at the pile head: (a) velocity admittance; (b) reflected wave signal

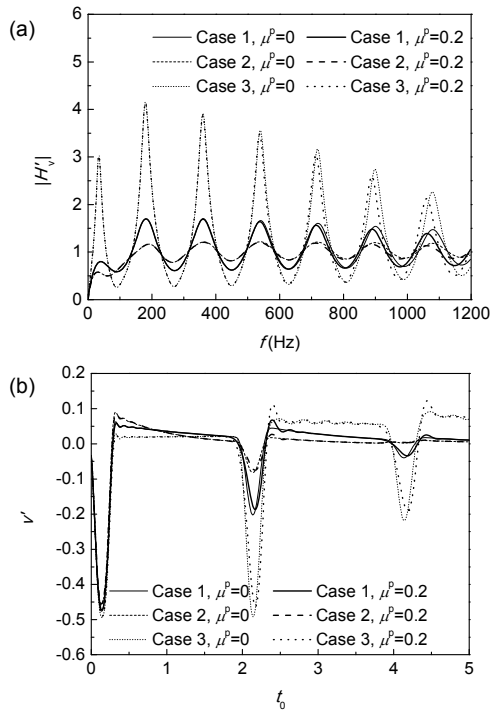

Fig. 5 Relationship between the transverse inertia effect of the pile and the radial inhomogeneity of the surrounding soil: (a) velocity admittance; (b) reflected wave signal

Case b: $\rho_k^s=\left[1800+100(m-k)/(m-1)\right]$ kg/m^3,

$v_k^s=\left[150+100(m-k)/(m-1)\right]$ m/s;

Case c: $\rho_k^s=\left[1800+150(m-k)/(m-1)\right]$ kg/m^3,

$v_k^s=\left[150+150(m-k)/(m-1)\right]$ m/s.

Fig. 6 shows the influence of the transverse inertia effect on the dynamic response at the pile head with different strengthening degrees of the surrounding soil in the radial direction. It can be noted from Fig. 6a that with the increase of the strengthening degree of the surrounding soil, the oscillation amplitude of the velocity admittance decreases, and the decrease rate of the resonant frequencies becomes slightly less notable. Fig. 6b shows that the influence of the transverse inertia effect tends to be weakened gradually with the increase of the strengthening degree of the surrounding soil.

4.2.3 Influence of the weakening degree of the surrounding soil

In this section, the soil parameters decrease radially inwards from the outmost zone in three cases, viz. cases A, B, and C, in which the weakening degree of the soil increases. The outer radius of the disturbed region is 0.5 m. In the three cases, parameters of each soil zone are set as

Case A: $\rho_k^s=\left[1800-30(m-k)/(m-1)\right]$ kg/m^3,

$v_k^s=\left[150-30(m-k)/(m-1)\right]$ m/s;

Case B: $\rho_k^s=\left[1800-60(m-k)/(m-1)\right]$ kg/m^3,

$v_k^s=\left[150-60(m-k)/(m-1)\right]$ m/s;

Case C: $\rho_k^s=\left[1800-90(m-k)/(m-1)\right]$ kg/m^3,

$v_k^s=\left[150-90(m-k)/(m-1)\right]$ m/s.

As shown in Fig. 7, as the weakening degree of the surrounding soil increases, both the decreasing trend of the resonant frequencies of the velocity admittance and the delay of the reflected signal from the pile tip become more apparent.

4.2.4 Influence of the strengthening range of the surrounding soil

In the following analysis, the mass density and shear wave velocity of the outer undisturbed soil zone are 1800 kg/m^3 and 150 m/s, and increase linearly

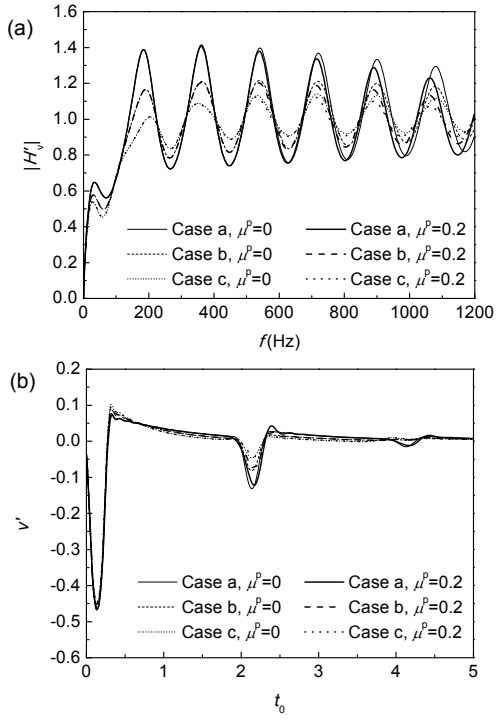

Fig. 6 Influence of the strengthening degree of the surrounding soil on the dynamic response at the pile head: (a) velocity admittance; (b) reflected wave signal

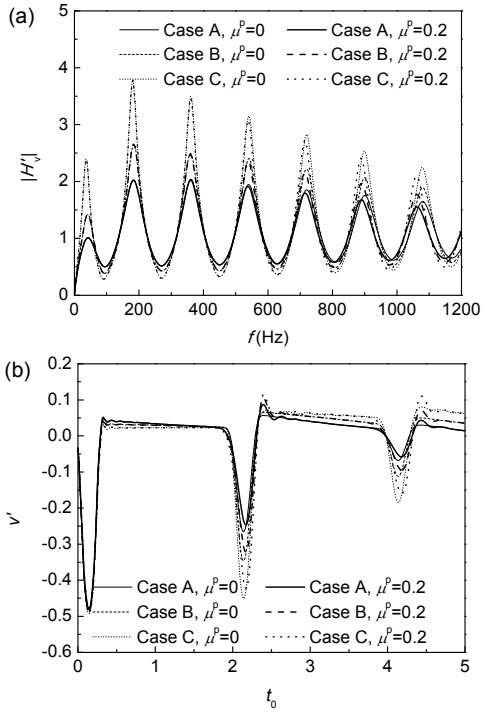

Fig. 7 Influence of the weakening degree of the surrounding soil on the dynamic response at the pile head: (a) velocity admittance; (b) reflected wave signal

radially inwards to 1850 kg/m^3 and 200 m/s, respectively; the strengthening range of the surrounding soil is b=0 m, 0.25 m, or 0.5 m, in which b=0 m means that the soil is radially homogeneous.

Fig. 8 shows the influence of the transverse inertia effect on the dynamic response at the pile head with different strengthening ranges of the surrounding soil. It can be noted from Fig. 8a that as the strengthening range of the surrounding soil increases, the oscillation amplitude of the velocity admittance decreases. However, when the strengthening range reaches to 0.25 m, its further increase has little influence on the velocity admittance especially in the high frequency domain, which means that the soil adjacent to the pile has more influence on the dynamic characteristics of the pile than that of the far-field. This principle can also be supported by the decrease of the amplitude of the reflected signal shown in Fig. 8b. It can also be seen that the influence degree of the transverse inertia effect has a slight decrease with the increase of the strengthening range of the surrounding soil.

4.2.5 Influence of the weakening range of the surrounding soil

In this section, the mass density and the shear wave velocity of the outer undisturbed soil zone are 1800 kg/m^3 and 150 m/s, and decrease linearly radially inwards to 1750 kg/m^3 and 100 m/s, respectively; the weakening range of the surrounding soil is b=0 m, 0.25 m, or 0.5 m.

Fig. 9 also shows that it is the soil adjacent to the pile that greatly affects the dynamic characteristics of the pile rather than that of the far-field. In addition, the influence degree of the transverse inertia effect has a slight increase as the weakening range of the surrounding soil increases.

5 Comparison with other solutions

Li *et al.* (2005) conducted an *in situ* test by using the low strain reflected wave method to detect the length of a large diameter end-bearing pile. The equipment used for this test included a portable

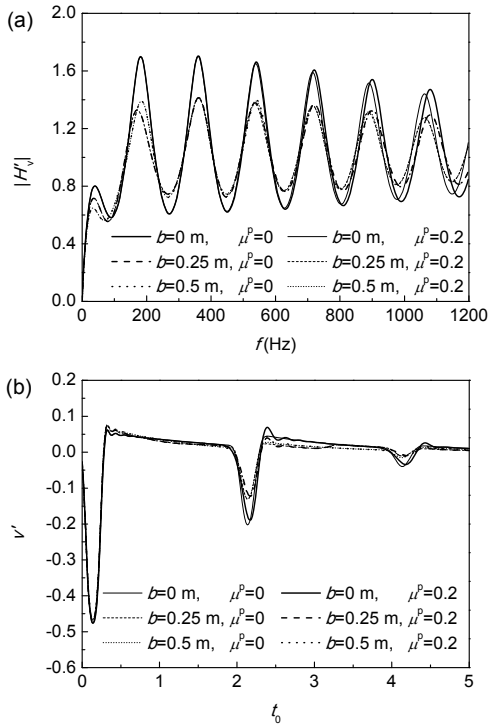

Fig. 8 Influence of the strengthening range of the surrounding soil on the dynamic response at the pile head: (a) velocity admittance; (b) reflected wave signal

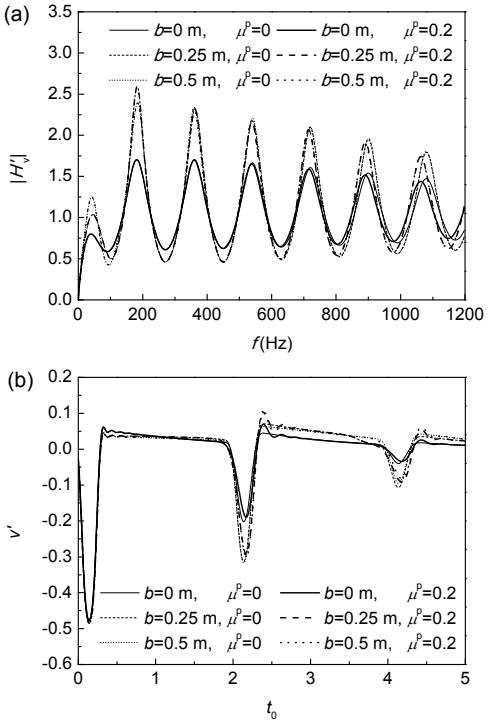

Fig. 9 Influence of the weakening range of the surrounding soil on the dynamic response at the pile head: (a) velocity admittance; (b) reflected wave signal

computer equipped with a data acquisition board and signal conditioning card, an accelerometer, and a small handheld hammer. Before the test, the pile head was cleaned and leveled. The schematic of the test is shown in Fig. 10. First, the accelerometer connected to the computer is placed on the pile head. Then, the handheld hammer is used to impact the pile head to produce a longitudinal low-strain stress wave that transmits along the pile shaft. Finally, the reflected signal containing the information of pile length and pile integrity is captured by the accelerometer and transmitted to the computer. Soil-pile parameters are shown as follows: length, diameter, longitudinal wave velocity, and Poisson's ratio of the pile are 5.1 m, 1 m, 3500 m/s, and 0.25, respectively; shear modulus and Poisson's ratio of the surrounding soil are 42.9 MPa and 0.45, respectively.

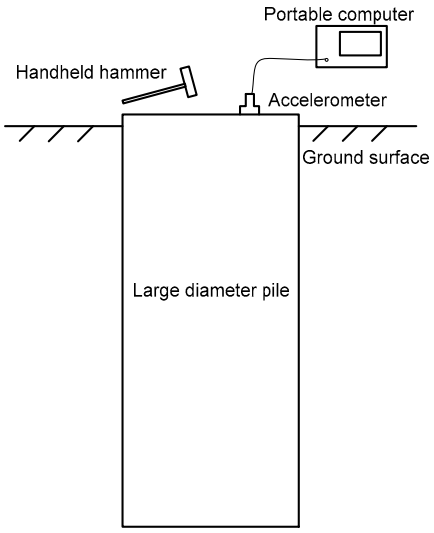

Fig. 10 Schematic of the field test

The calculated curve is derived based on the solution proposed in this paper, and is compared with the measured curve and those obtained by other solutions. As shown in Fig. 11, the peak times of the calculated reflected signals given in this paper and Li *et al*. (2005) are consistent, and agree well with the measured result, demonstrating that the time lag of the reflected signal (i.e., the decrease of the wave velocity) caused by the dispersion effect of the large diameter pile can be approximately reflected by considering its transverse inertia effect. It can also be seen that if the decrease of the wave velocity is not considered, the pile length calculated by the peak-to-peak method will be longer than its actual value, and the error is about 0.2 m, which cannot be neglected for a 5.1-m long pile. As the material damping of the pile is not considered, the amplitude of the reflected signal in Li *et al.* (2005)'s calculated curve is much bigger and the oscillation following the reflected signal is much stronger than that for this paper and the measured result. In addition, such limiting assumptions as homogeneous soil and a fixed pile tip made by Li *et al.* (2005) can be overcome by the solution proposed in this paper.

The obvious oscillation of the measured curve can be observed now to be around t=0.5 ms while this phenomenon is not notable in the calculated curves. As the pile hole is artificially dug and the pile is quite short, the cross section of the pile shaft is less likely changed. As a result, the oscillation of the measured curve may be caused by the factors during the test, such as the materials of the handheld hammer and the position of the accelerometer. After all, it does not interfere with the detection of the pile length.

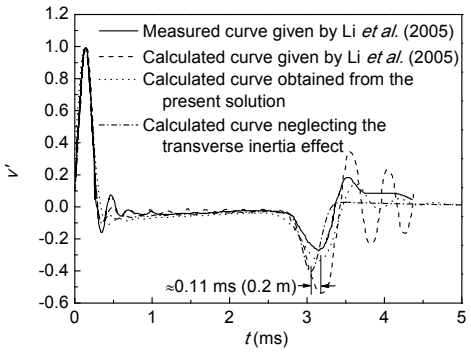

Fig. 11 Comparison of the calculated results and the measured result

6 Conclusions

By utilizing the 3D axisymmetric model presented in this paper, the analytical solution in the frequency domain and the semi-analytical solution in the time domain of the vertical vibration of a large diameter pile embedded in inhomogeneous soil are obtained by considering its transverse inertia effect. A parametric analysis is conducted to investigate the influence of the transverse inertia effect on the dynamic response of the pile and its relationship with the pile parameters and the radial inhomogeneity of the surrounding soil.

When considering the transverse inertia effect, the decrease of the resonant frequencies of the velocity admittance is observed and becomes greater for higher frequencies. The influence on the dynamic response in the time domain is mainly shown in such aspects as the impulse width increase, the amplitude decrease, and the time lag of the reflected signal from the pile tip as well as the appearance of the oscillation after the reflected signal. It is worth noting that the delay of the reflected signal from the pile tip may lead to the overestimation of the pile length, which to some extent, interferes with the dynamic testing of the pile.

The influence of the transverse inertia effect on the dynamic response at the pile head is affected by pile parameters and the radial inhomogeneity of the pile surrounding soil. To be specific, the influence degree increases with the increase of the pile radius, Poisson's ratio, weakening range, and weakening degree of the pile surrounding soil, while it decreases with the increase of the concrete strength grade of the pile, the strengthening range and strengthening degree of the pile surrounding soil.

Comparison with the measured results and two other calculated results shows that the proposed model is effective to simulate the vertical vibration of a large diameter pile.

References

Achenbach, J.D., 1973. Wave Propagation in Elastic Solids. Elsevier, the Netherland.

Chai, H.Y., Phoon, K.K., Zhang, D.J., 2010. Effects of the source on wave propagation in pile integrity testing. *Journal of Geotechnical and Geoenvironmental Engineering*, **136**(9):1200-1208. http://dx.doi.org/10.1061/(ASCE)GT.1943-5606.0000272

Chai, H.Y., Wei, C.F., Phoon, K.K., *et al.*, 2011. Some observations on the performance of the signal matching technique in assessment of pile integrity. *Journal of Nondestructive Evaluation*, **30**(4):246-258. http://dx.doi.org/10.1007/s10921-011-0113-9

Chow, Y.K., Phoon, K.K., Chow, W.F., *et al.*, 2003. Low strain integrity testing of piles: 3D effects. *Journal of Geotechnical and Geoenvironmental Engineering*, **129**(11):1057-1062. http://dx.doi.org/10.1061/(ASCE)1090-0241(2003)129:11(1057)

Ding, X.M., Liu, H.L., Liu, J.Y., *et al.*, 2011. Wave propagation in a pipe pile for low-strain integrity testing. *Journal of Engineering Mechanics*, **137**(9):598-609. http://dx.doi.org/10.1061/(ASCE)EM.1943-7889.0000263

El Naggar, M.H., 2000. Vertical and torsional soil reactions for radially inhomogeneous soil layer. *Structural Engineering and Mechanics*, **10**(4):299-312. http://dx.doi.org/10.12989/sem.2000.10.4.299

El Naggar, M.H., Novak, M., 1994. Nonlinear axial interaction in pile dynamics. *Journal of Geotechnical Engineering*, **120**(4):678-696. http://dx.doi.org/10.1061/(ASCE)0733-9410(1994)120:4(678)

El Naggar, M.H., Wei, J.Q., 2000. Uplift behaviour of tapered piles established from model tests. *Canadian Geotechnical Journal*, **37**(1):56-74. http://dx.doi.org/10.1139/t99-090

Elkasabgy, M., El Naggar, M.H., 2013. Dynamic response of vertically loaded helical and driven steel piles. *Canadian Geotechnical Journal*, **50**(5):521-535. http://dx.doi.org/10.1139/cgj-2011-0126

Gong, C.Z., He, C.L., Gong, W.M., *et al.*, 2012. Analysis of size effect on large diameter rock-socketed pile based on self-balance method. *Rock and Soil Mechanics*, **33**(8):2403-2407 (in Chinese).

Han, Y.C., 1997. Dynamic vertical response of piles in nonlinear soil. *Journal of Geotechnical and Geoenvironmental Engineering*, **123**(8):710-716. http://dx.doi.org/10.1061/(ASCE)1090-0241(1997)123:8(710)

Han, Y.C., Sabin, G.C.W., 1995. Impedances for radially inhomogeneous viscoelastic soil media. *Journal of Engineering Mechanics*, **121**(9):939-947. http://dx.doi.org/10.1061/(ASCE)0733-9399(1995)121:9(939)

He, C.L., Gong, C.Z., Gong, F., *et al.*, 2015. Laboratory test on the effect of diameter and depth of rock-socketed piles. *Chinese Journal of Underground Space and Engineering*, **11**(2):293-298 (in Chinese).

Jardine, R.J., Zhu, B.T., Foray, P., *et al.*, 2013. Measurement of stresses around closed-ended displacement piles in sand. *Géotechnique*, **63**(1):1-17. http://dx.doi.org/10.1680/geot.9.P.137

Li, Q., Wang, K.H., Xie, K.H., 2005. Dynamic response for vertical vibration of large diameter pile in saturated soil. *Journal of Vibration Engineering*, **18**(4):500-505 (in Chinese).

Li, Z.Y., Wang, K.H., Lv, S.H., *et al.*, 2015. A new approach for time effect analysis in the settlement of single pile in nonlinear viscoelastic soil deposits. *Journal of Zhejiang University-SCIENCE A (Applied Physics & Engineering)*, **16**(8):630-643. http://dx.doi.org/10.1631/jzus.A1400329

Liao, S.T., Roesset, J.M., 1997. Dynamic response of intact piles to impulse loads. *International Journal for Numerical and Analytical Methods in Geomechanics*, **21**(4):255-275. http://dx.doi.org/10.1002/(SICI)1096-9853(199704)21:4<255::AID-NAG869>3.0.CO;2-J

Liu, F.T., Zhao, C.F., Wu, J., *et al.*, 2010. Experimental research on bearing behavior and size effect of large diameter bored cast-*in-situ* piles in Changzhou area. *Chinese Journal of Rock Mechanics and Engineering*,

29(4):858-864 (in Chinese).

Lü, S.H., Wang, K.H., Wu, W.B., *et al.*, 2014. Longitudinal vibration of a pile embedded in layered soil considering the transverse inertia effect of pile. *Computers and Geotechnics*, **62**:90-99. http://dx.doi.org/10.1016/j.compgeo.2014.06.015

Lü, S.H., Wang, K.H., Wu, W.B., *et al.*, 2015. Longitudinal vibration of pile in layered soil based on Rayleigh-Love rod theory and fictitious soil-pile model. *Journal of Central South University*, **22**(5):1909-1918. http://dx.doi.org/10.1007/s11771-015-2710-8

Militano, G., Rajapakse, R.K.N.D., 1999. Dynamic response of a pile in a multi-layered soil to transient torsional and axial loading. *Géotechnique*, **49**(1):91-109. http://dx.doi.org/10.1680/geot.1999.49.1.91

MOHURD (Ministry of Housing and Urban-Rural Development), 2010. Code for Design of Concrete Structures, GB50010-2010. China Architecture & Building Press, China (in Chinese).

Nogami, T., Novák, M., 1976. Soil-pile interaction in vertical vibration. *Earthquake Engineering & Structural Dynamics*, **4**(3):277-293. http://dx.doi.org/10.1002/eqe.4290040308

Nogami, T., Konagai, K., 1988. Time domain flexural response of dynamically loaded single piles. *Journal of Engineering Mechanics*, **114**(9):1512-1525. http://dx.doi.org/10.1061/(ASCE)0733-9399(1988)114:9(1512)

Que, R.B., Wang, K.H., 2007. Theory on longitudinal vibration of pile in viscous damping soil layer considering 3D wave effect and its applications. *Chinese Journal of Rock Mechanics and Engineering*, **26**(2):381-390 (in Chinese).

Randolph, M.F., Deeks, A.J., 1992. Dynamic and static soil models for axial pile response. Proceedings of the 4th International Conference on the Application of Stress Wave Theory to Piles, the Hague, the Netherlands, p.21-24.

Seidel, J.P., Tan, S.K., 2004. Elimination of the Rayleigh wave effect on low strain integrity test results (Part 1: experimental investigation). Proceedings of the 7th International Conference on the Application of Stress Wave Theory to Piles, Kuala Lumpur, Malaysia, p.179-185.

Tian, X.J., Hu, W.T., Gong, X.N., 2015. Longitudinal dynamic response of pile foundation in a nonuniform initial strain field. *KSCE Journal of Civil Engineering*, **19**(6):1656-1666. http://dx.doi.org/10.1007/s12205-014-0049-6

Wang, N., Wang, K.H., Wu, W.B., 2013. Analytical model of vertical vibrations in piles for different tip boundary conditions: parametric study and applications. *Journal of Zhejiang University-SCIENCE A (Applied Physics & Engineering)*, **14**(2):79-93. http://dx.doi.org/10.1631/jzus.A1200184

Wu, W.B., Wang, K.H., Yang, D.Y., *et al.*, 2012. Longitudinal dynamic response to the pile embedded in layered soil based on the fictitious soil pile model. *Chinese Journal of Highway and Transport*, **25**(2):72-80 (in Chinese).

Wu, W.B., Wang, K.H., Zhang, Z.Q., *et al.*, 2013. Soil-pile interaction in the pile vertical vibration considering true three-dimensional wave effect of soil. *International Journal for Numerical and Analytical Methods in Geomechanics*, **37**(17):2860-2876. http://dx.doi.org/10.1002/nag.2164

Wu, W.B., Jiang, G.S., Huang, S.G., *et al.*, 2014. Vertical dynamic response of pile embedded in layered transversely isotropic soil. *Mathematical Problems in Engineering*, **2014**(12):1-12. http://dx.doi.org/10.1155/2014/126916

Yang, D.Y., Wang, K.H., Ding, H.P., 2013. Vertical vibration of pile based on continuum medium model in vertically and radially inhomogeneous soil layers. *China Civil Engineering Journal*, **46**(3):119-126 (in Chinese).

Yang, X., Tang, J., 2013. Vertical vibration of single pile with transversal inertia effect in stratified saturated soil. *Rock and Soil Mechanics*, **34**(6):1560-1566 (in Chinese).

Yesilce, Y., Catal, H.H., 2008a. Free vibration of piles embedded in soil having different modulus of subgrade reaction. *Applied Mathematical Modelling*, **32**(5):889-900. http://dx.doi.org/10.1016/j.apm.2007.02.015

Yesilce, Y., Catal, H.H., 2008b. Free vibration of semi-rigid connected Reddy-Bickford piles embedded in elastic soil. *Sadhana-Academy Proceedings in Engineering Sciences*, **33**(6):781-801. http://dx.doi.org/10.1007/s12046-008-0034-1

Yesilce, Y., Catal, H.H., 2008c. Free vibration of semi-rigidly connected piles embedded in soils with different subgrades. *International Journal of Structural Stability and Dynamics*, **8**(2):299-320. http://dx.doi.org/10.1142/S0219455408002661

Yu, J., Cai, Y.Y., Wu, W.B., 2013. Effect of sediment on vertical dynamic impedance of rock-socketed pile with large diameter. *Journal of Central South University*, **20**:2856-2862. http://dx.doi.org/10.1007/s11771-013-1806-2

Zhou, J.J., Wang, K.H., Gong, X.N., *et al*., 2013. Bearing capacity and load transfer mechanism of a static drill rooted nodular pile in soft soil areas. *Journal of Zhejiang University-SCIENCE A (Applied Physics & Engineering)*, **14**(10):705-719. http://dx.doi.org/10.1631/jzus.A1300139

Zhou, J.J., Gong, X.N., Wang, K.H., *et al.*, 2015. A field study on the behavior of static drill rooted nodular piles with caps under compression. *Journal of Zhejiang University-SCIENCE A (Applied Physics & Engineering)*, **16**(12):951-963. http://dx.doi.org/10.1631/jzus.A1500168

Zhou, X.L., Wang, J.H., Jiang, L.F., *et al*., 2009. Transient dynamic response of pile to vertical load in saturated soil. *Mechanics Research Communications*, **36**(5):618-624. http://dx.doi.org/10.1016/j.mechrescom.2009.01.004

中文概要

题　目： 基于 Rayleigh-Love 杆理论的非均质土中大直径桩纵向振动

目　的： 研究大直径桩横向惯性效应对其动力响应的影响以及与土体径向非均质性的关系。

创新点： 1. 采用 Rayleigh-Love 杆模型模拟大直径桩，考虑其横向惯性效应；2. 所建立的桩土相互作用模型能同时考虑土体的竖向成层性和径向非均质性。

方　法： 1. 采用 Rayleigh-Love 杆模型模拟大直径桩，建立桩土体系纵向振动控制方程（公式（1）和（4））；2. 通过求解方程，得到桩顶纵向振动频域响应解析解（公式（15））和时域响应半解析解（公式（16））；3. 通过参数分析的方法，研究横向惯性效应对桩顶响应的影响以及与桩身参数和桩周土径向非均质性的关系（图 2~9）；4. 通过与工程实例的对比，证明本文解的合理性（图 11）。

结　论： 1. 考虑横向惯性效应时，桩底反射信号后移，导致桩的计算长度大于其实际值；2. 横向惯性效应的影响程度随着桩身半径、泊松比、桩周土软化范围和软化程度的增大而增强，随着桩身混凝土强度等级、桩周土硬化范围和硬化程度的增大而减弱；3. 考虑横向惯性效应时的计算曲线与实测曲线更为吻合。

关键词： 大直径桩；纵向振动；横向惯性效应；Rayleigh-Love 杆模型；非均质土